Microstructure evolution of commercial pure titanium during equal channel angular pressing

Y.J. Chen [a,*], Y.J. Li [b], J.C. Walmsley [b], S. Dumoulin [b], P.C. Skaret [a], H.J. Roven [a]

[a] The Norwegian University of Science and Technology, Department of Materials Science and Engineering, 7491 Trondheim, Norway
[b] SINTEF, Materials and Chemistry, 7465 Trondheim, Norway

a b s t r a c t

The microstructure development of commercially pure titanium during 3 and 4 passes of equal channel angular pressing (ECAP) has been investigated in detail by optical microscopy and electron backscattered diffraction (EBSD). The flow line, texture, grain, subgrain and twinning structures along the whole length of the ECAP bar have been characterized systematically. A theoretically predicted triangular zone with a completely different flow line pattern and texture has been found at the extruded end of the sample. Details of the misorientation gradient inside grains and the continuous dynamic recrystallization (CDRX) mechanism are discussed. Low angle grain boundaries (LAGBs) in grains are seen to evolve into high angle grain boundaries (HAGBs) throughout the material. No $\{1\,0\,\bar{1}\,1\}$ twinning was detected but a low fraction of $\{1\,0\,\bar{1}\,2\}$ twins was present.

Keywords:
Electron backscatter diffraction (EBSD)
Equal channel angular pressing (ECAP)
Commercially pure (CP) Ti
Continuous dynamic recrystallization (CDRX)
Grain boundary

(1) Introduction

Titanium alloys, e.g. Ti6Al4V, have increasing applications in biomedical devices due to their excellent mechanical and biological performance [1]. Alloying elements such as Al and V are toxic and may potentially cause a series of ailments including cancer [2]. Thus the use of commercially pure (CP) Ti would be desirable. However, coarse-grained CP Ti usually has limited strength which cannot meet the needs for medical implants. An effective tactic to minimize this disadvantage is to develop nanostructured or ultrafine-grained (UFG) CP Ti.

Equal channel angular pressing (ECAP), aimed at the fabrication of massive bulk nanostructured materials (NSM) or UFG materials, has been successfully used to obtain UFG and even NSM microstructures from Al, Cu, Ni, Ti, steel, Mg and their alloys [3–8]. The deformation behavior and grain refinement mechanism of relatively soft alloys with FCC structures, e.g. Al and Cu, have been studied extensively [4,9]. In the last years, there has been increasing interest in investigating hard to form metals or alloys, e.g. Ti, with hexagonal close packed (HCP) structure processed by ECAP [10–14]. In order to obtain the finest grain size, ECAP at low temperature is a promising solution. Zhao et al. [10] recently observed shear bands with irregular cell structures and deformation twins of $\{1\,0\,\bar{1}\,1\}$ type in the microstructure of CP Ti after 1 ECAP pass with 120° die at room temperature. ECAP plus cold deformation [2,11] can further refine the grains and improve the strength. Shin et al. [12] have reported that the main deformation mechanisms of CP Ti during the first and the second ECAP pass at 623 K are $\{1\,0\,\bar{1}\,1\}$ twinning and dislocation slip. However, no attempt was made to study the twin types for subsequent ECAP passes. Zhu et al. [14] systematically characterized the hierarchy of defect structures in nanostructured Ti. However, they did not study the grain refinement mechanism. In our previous work [13], the deformation structure including dislocation tangle zones (DTZ), dislocation cells (DC), twins and subgrains were investigated by electron backscattered diffraction (EBSD) and transmission electron microscopy (TEM) in the central region of the shear zone of a CP Ti sample interrupted between 3 and 4 ECAP passes. The objective of the present paper is to study the microstructure evolution of CP Ti during the 3rd and 4th pass to clarify the deformation mechanism beyond the first ECAP pass where $\{1\,0\,\bar{1}\,1\}$ twinning seems to dominate.

(2) Experimental procedure

Grade 2 CP Ti was used in the as-delivered condition, i.e. rolled and annealed at 977 K for 2 h followed by air cooling. Its composition (wt.%) was Fe 0.04, C 0.01, N 0.019, O 0.12 and H 0.001. In the annealed condition this material has a yield strength of 365 MPa. ECAP was performed via route A [15] at 723 K using 100 mm × 19.5 mm × 19.5 mm bars with an L-shaped split-die with

* Corresponding author. Tel.: +47 73594881; fax: +47 73590203.
E-mail address: happywinner01@gmail.com (Y.J. Chen).

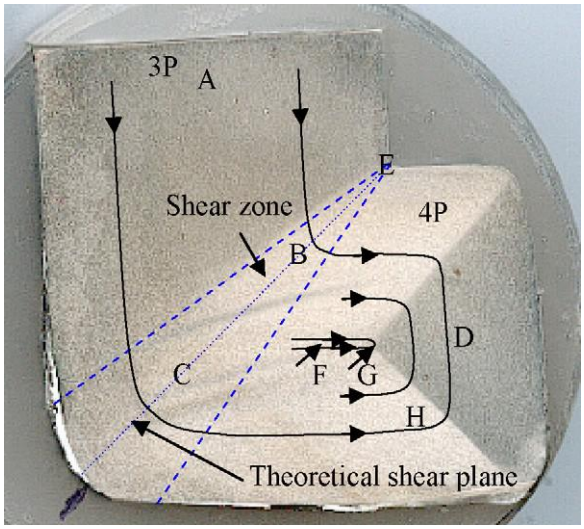

Fig. 1. Optical micrograph of CP Ti sample cross-section after 3/4 ECAP passes. The upper left is 3 passes and the lower right is 4 passes. This image is in mirror orientation with respect to subsequent images.

$\phi = 90°$ and $= 20.6°$ [16,17], which geometry leads to an imposed strain of about 1 per pass [18]. Repeated pressings were conducted and eventually interrupted during the 4th pass in order to observe the microstructure evolution from the 3rd to 4th pass. After processing, longitudinal sections of the sample were prepared for optical microscopy (OM) and EBSD analyses. The sample after 3/4 ECAP passes is shown in Fig. 1.

Samples for the EBSD study were prepared by mechanical grinding, mechanical polishing and final electropolishing with an AC3 solution, using a voltage of 40 V for 15–25 s under a controlled temperature of $-30\,°C$. Finally, the samples were cleaned with methanol. The EBSD collection was done in a Zeiss 55VP FEG-SEM equipped with a Nordif EBSD detector and the TSL OIM EBSD software. EBSD was performed at 20 kV, 20 mm working distance, a tilt angle of 70° and a scan step of 0.1 μm.

(3) Results

- Optical microstructures

Fig. 1 shows the CP Ti sample after 3/4 ECAP passes. Five positions, labelled A, B, C, D and H, were selected for further EBSD observation. Points B and C are located along the theoretical shear plane in the shear zone [19]. Positions A, E, F and G were selected for OM observation. The overall pass-to-pass development of flow lines is indicated by a black arrowed line. Images with higher magnifications are shown in Fig. 2 and these have a mirror orientation to Fig. 1. The white arrowed lines in Fig. 2 roughly follow the direction of flow lines. In the 3 passes region, shown in Fig. 2a, there is an overall deviation angle, relative to the ECAP channel axis, which is in agreement with the calculated value of 9.5° between the grain elongation direction and extrusion axis for the 3rd pass of route A [20]. Fig. 2b shows that flow lines near the inner angle ϕ [16,17] have a small radius of curvature, which increases from the corner to the center of the bar. The flow lines gradually change to being parallel to the horizontal direction, Fig. 2c, and display a horizontal "U" shaped change of direction at position G (Fig. 2d). It should be noted that the flow lines close to the outer surfaces are complicated due to the effect of friction. Fig. 1 clearly shows that there is a sharply defined triangular zone in the 4 passes section that includes position D, where the flow lines are almost perpendicular to the ECAP channel axis. This has not been reported in regard to CP Ti but is in good agreement with an earlier modeling study [21].

The formation of the triangular zone is attributed to the accumulated plastic flow in the outgoing specimen section moving from one pass to the next passes, as schematically shown in Fig. 3. There is a uniform deformation zone and two non-uniform zones after 1

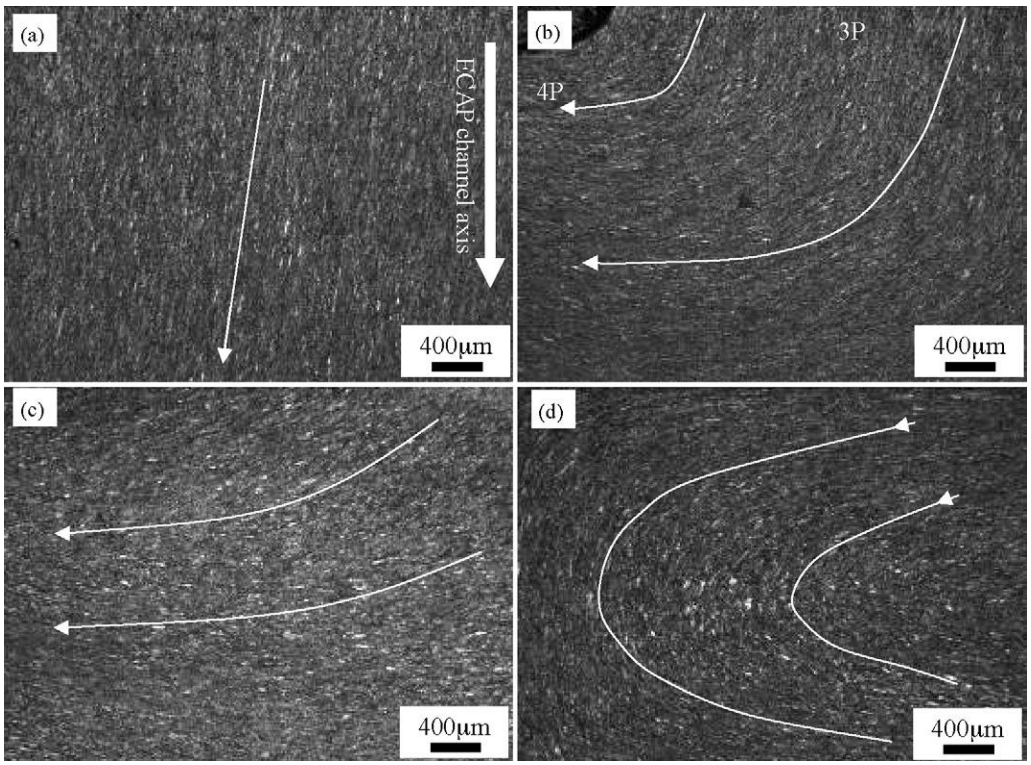

Fig. 2. Optical microstructures of positions (a) A, (b) E, (c) F and (d) G.

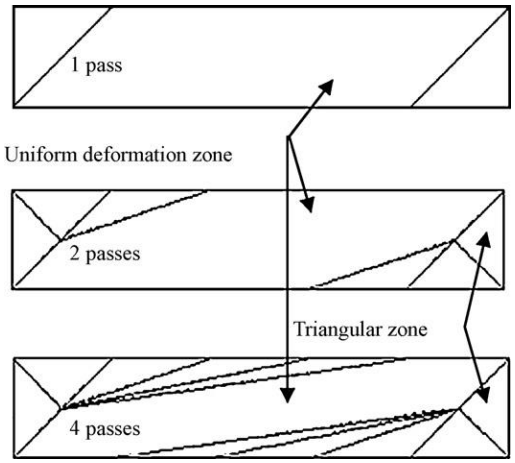

Fig. 3. Schematic showing the formation of triangle zone for ECAP route A.

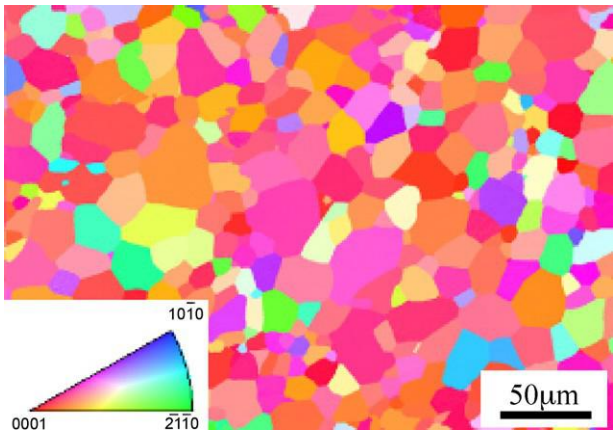

Fig. 4. Orientation map (SEM-EBSD) of as-rolled CP Ti.

ECAP pass. After the 2nd ECAP pass, the triangular zone forms at the end of the bar through the interaction of non-uniform deformation zones of the first and the second pass. With further ECAP passes the triangular zone remains at the same position in the specimen. The size of the triangular zone is expected to be affected by the length-to-thickness ratio of the bar and the material structure [21].

- EBSD microstructures

The initial (before ECAP) misorientation map is presented in Fig. 4. The color code, red for {0 0 0 1}, blue for $\{1\,0\,\bar{1}\,0\}$ and green for $\{2\,\bar{1}\,\bar{1}\,0\}$, gives the crystallographic direction of each grain. Equiaxed grains, with an average size of 21.6 μm are present. There is a high fraction of high angle grain boundaries (HAGBs, ~85%) and the average misorientation is 42.9°.

EBSD orientation maps of the sample after ECAP processing are shown in Fig. 5 (the map of point H is not shown here). The typical microstructures consist of elongated coarse grains and fine-grained band structures. At position A in the 3rd pass region, Fig. 5a, the longitudinal directions of the bands have an overall tilt relative to the ECAP channel axis, which is consistent with the results revealed by OM shown in Fig. 2a and the theoretical angle of 9.5°. Comparing the microstructures at locations B, C and D to that at location A, it

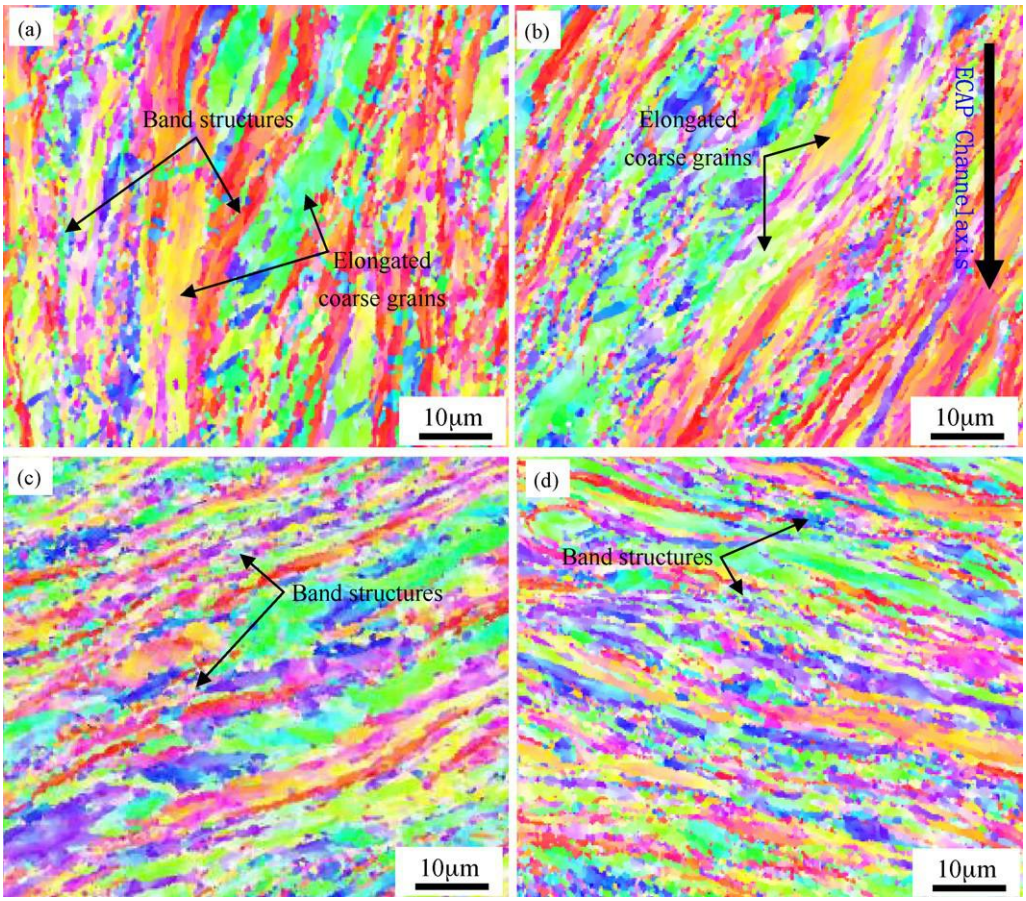

Fig. 5. Orientation maps (SEM-EBSD) of CP Ti after 3/4 ECAP passes at 723 K. (a) Point A, (b) point B, (c) point C and (d) point D.

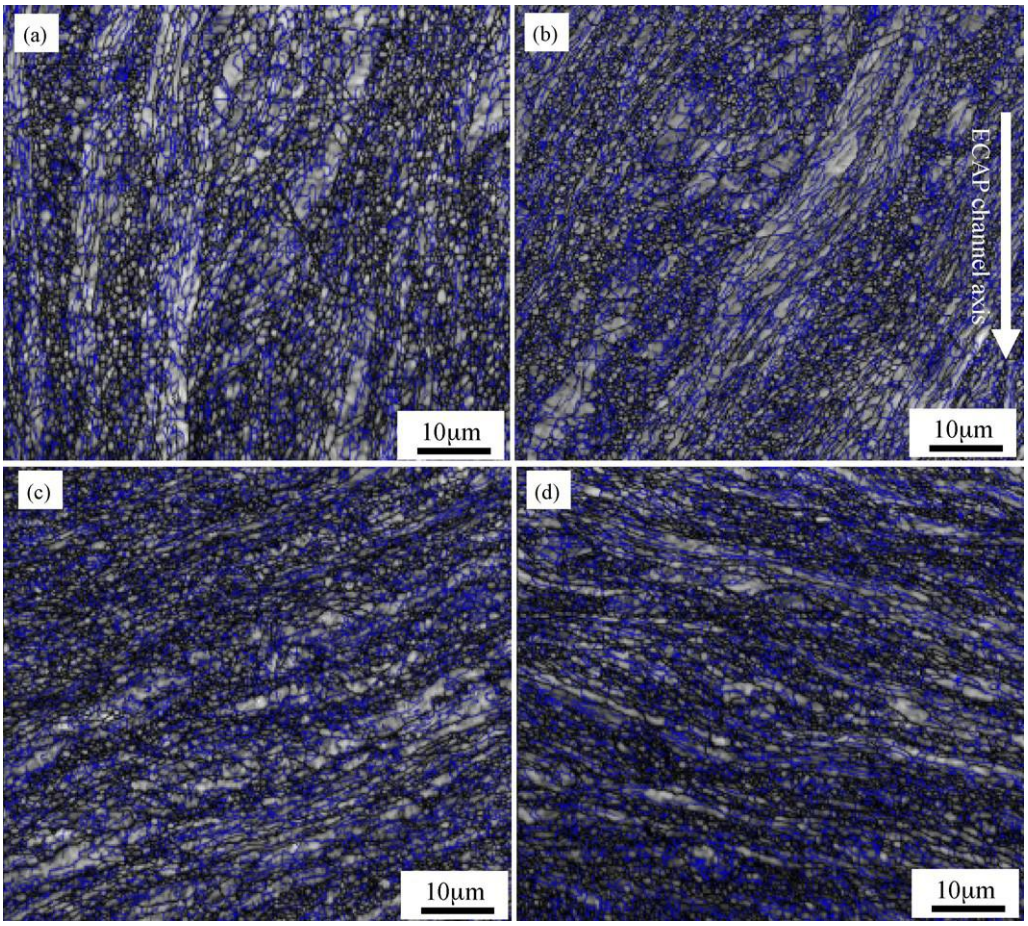

Fig. 6. Grain boundary maps (SEM-EBSD) of CP Ti after 3/4 ECAP passes at 723 K. (a) Point A, (b) point B, (c) point C and (d) point D.

can be seen that the average thickness of the bands is lower, showing that the band structures are further refined when the material passes through the shear zone in the ECAP die.

Fig. 6 presents the grain boundary maps derived from the orientation EBSD maps in Fig. 5. The low angle grain boundaries (LAGBs), between 2° and 15°, and the HAGBs, beyond 15°, are marked by thin blue lines and thick black lines, respectively. Grain boundaries with misorientations below 2° are removed due to the resolution limit of EBSD. It is seen that a large number of necklace-like ultrafine equiaxed grains have formed along the boundaries of the band structures. As shown in Fig. 6a–d, and discussed in greater detail below, the ultrafine grains at locations B and C are finer than those at location A. Elongated coarse grains can still be observed, within which are distributed many ultrafine subgrains, bounded by LAGBs. These band structures tend to be aligned parallel with each other but intersect at local zones. The thickness of the fine-grained band structures varies between 1 grain and about 10 grains. By comparing Fig. 6b and c with Fig. 6a, it can be seen that the fine grains are further refined when the material passes through points B and C in the shear plane. The average spacing between fine-grained band structures also decreases from point A to D.

The fractional total lengths of HAGBs and LAGBs at different locations have been measured from the EBSD maps, Table 1. The fraction of HAGBs is low relative to other UFG materials processed by SPD, for example Mg alloys [22]. After passing through the shear plane, both the actual length of the HAGBs and LAGBs are larger than that in the microstructure of the 3rd pass region, showing further refinement of both grains and sub grains during the 4th ECAP pass. Table 1 indicates that the density of dislocation substructures with low misorientations (typical less than 5°) increases when the material passes through the shear plane, points B and C, which indicates that dislocation slip is the dominant deformation mechanism during 3 and 4 ECAP passes.

Fig. 7 displays typical distribution histograms of grain size after 3/4 ECAP processing. The average grain size after 3 ECAP passes is about 0.8 μm, Fig. 7a. During shear deformation, the fraction of both fine and coarse grains tends to increase, as can be seen in Fig. 7b and c, consistent with the increase in total LAGB and HAGB length (Table 1). The final average grain size in the triangular zone reaches 0.65 μm, seen in Fig. 7d.

The misorientation angle distributions are shown in Fig. 8. No frequency peak is present around 56°, showing that there is no measurable level of $\{1\,0\,\bar{1}\,1\}$ twinning. This is in agreement with the observations of Shin et al. on CP Ti processed at 350 °C [12], where, no $\{1\,0\,\bar{1}\,1\}$ twinning could be found by transmission electron microscopy after 2 ECAP passes. In contrast, there is a significant frequency peak around a misorientation angle of 86° for both points A (3 passes) and H (4 passes but off the centre axis), marked by an arrow, that indicates the presence of $\{1\,0\,\bar{1}\,2\}$ twinning during the 3rd and the 4th passes of ECAP processing.

Table 1
Fraction (%) and actual length (mm) of HAGBs and LAGBs in Fig. 6.

Location	Fraction (%)			Actual length (mm)		
	2–5°	5–15°	15–180°	2–5°	5–15°	15–180°
Point	19.	25.7	54.5	6.1	6.97	16.9
Point	20.	27.7	51.6	7.3	9.84	18.3
Point	24.	23.4	52.4	8.3	8.14	18.2
Point	22.	23.6	53.9	8.0	8.44	19.3
D	5			5		

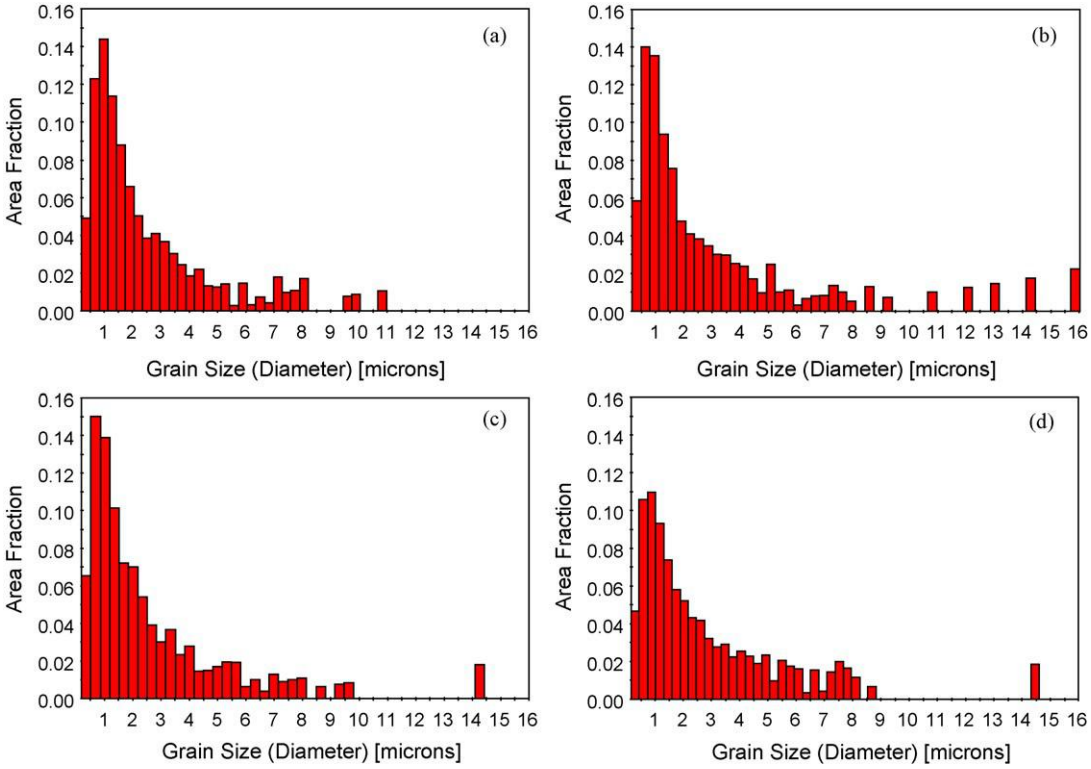

Fig. 7. Grain size distribution of CP Ti after 3/4 ECAP passes at 723 K. (a) Point A, (b) point B, (c) point C and (d) point D.

In our previous work [13], we have identified $\{1\,0\,\bar{1}\,2\}$ twins with width around 100 nm in the shear plane during 4th pass ECAP by using TEM and observed a similar peak to those in Fig. 8 in EBSD orientation distribution. However, twins with width of several microns, could be missed in TEM observation. In order to observe this big twins and to confirm that the peak in grain boundary misorientations around 86° is really due to $\{1\,0\,\bar{1}\,2\}$ twins, several individual boundaries were further studied by orientation and trace analysis. An example of the analysis is presented in Fig. 9. The highlighted boundary meets the two criteria suggested by Mason et al. [24] and Nave et al. [25] for a coherent twinning boundary. Firstly, the crystals on either side of the boundary have coincident $\{1\,0\,\bar{1}\,2\}$ plane normals and, secondly, these twin plane normals are coincident with the boundary trace normal, seen as the parallel green lines in Fig. 9a and b. The existence of $\{1\,0\,\bar{1}\,2\}$ twins indicates that the twinning has also contributed to deformation during both the 3rd and 4th passes, even though dislocation slip is dominant. The reason for the activation of $\{1\,0\,\bar{1}\,2\}$ tensile twins instead of $\{1\,0\,\bar{1}\,1\}$ compression twins needs to be further studied.

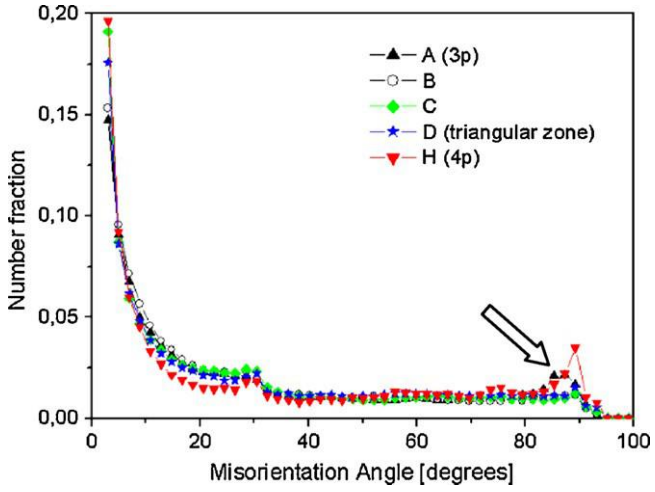

Fig. 8. Misorientation distribution (SEM-EBSD) of CP Ti during 3/4 ECAP passes.

Changes in the angle between the grain elongation direction and the extrusion axis with increasing number of passes by route A [20], will lead to the change of band structure and preferential grain texture during the shear deformation. Fig. 10 shows the evolution of $\{0\,0\,0\,1\}$ pole figures for the analysed positions shown in Fig. 1. Fig. 10a–c correspond to the orientation maps of Fig. 5a–c. Reconsidering Fig. 1, RD (reference direction) and TD (transverse direction) are parallel and perpendicular to the ECAP channel axis in the observation plane, respectively. For the microstructure of point A, in Fig. 10a, it is evident that there is a texture with the c-axis ($(0\,0\,0\,1)$ crystal direction) of grains being around 80° towards RD. During the shear deformation at position B, Fig. 10b, the c-axis rotates around the normal direction (ND), i.e. the axis defined by the pole figure centres. Fig. 10c shows that the c-axis of most grains in the triangular zone is around 80° towards TD. Fig. 10d shows that the angle between the c-axis and RD decreases in 4 passes of ECAP (point H) compared with that of 3 ECAP passes (Fig. 10a). On comparing the textures with the flow lines shown in Figs. 2 and 5, it is interesting to see that the basal planes of most crystals tend to be aligned parallel to the local flow lines. The present result indicates that the c-axis of most grains progressively rotate around the axis ND during 3/4 ECAP passes, i.e. from points A to D.

(4) Discussion

- Microstructure in triangular zone

In the present study, the triangular zone occupied a large proportion of the 4 passes part of the sample. No observation of

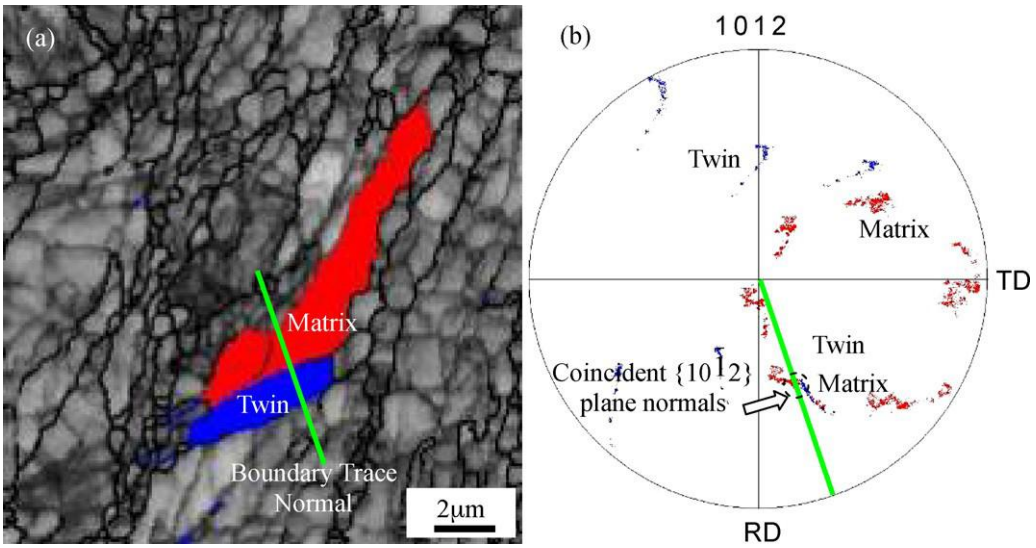

Fig. 9. EBSD analysis of{1 0 $\bar{1}$ 2}twins seen in the microstructure of CP Ti during 3/4 ECAP passes, taken from Fig. 6b. (a) Grain boundary map showing{1 0 $\bar{1}$ 2}twin boundaries (85.1°). A twin and the matrix are highlighted in blue and red, respectively. (b) The corresponding pole figure showing the twin interior orientation shares a common pole with the matrix, which is marked by arrow. (For interpretation of the references to color in this figure legend, the reader is referred to the web version of the article.)

microstructure in the triangular zone of ECAPed bars has been reported previously. Observations presented in Figs. 1 and 2, Figs. 5–8 and Fig. 10 show that the grain size and shape, fraction of LAGBs, misorientation distribution in the microstructure of point D are similar to other locations. However, the flow lines, the direction of band structures and the texture are different.

- Misorientation gradient inside individual grains

Fig. 11 shows a typical elongated coarse grain at point B, in the theoretical shear plane, highlighted by color contrast. As can be seen, there are several subgrains within the grain. In order to examine how the orientation varies in the highlighted grain, two lines are

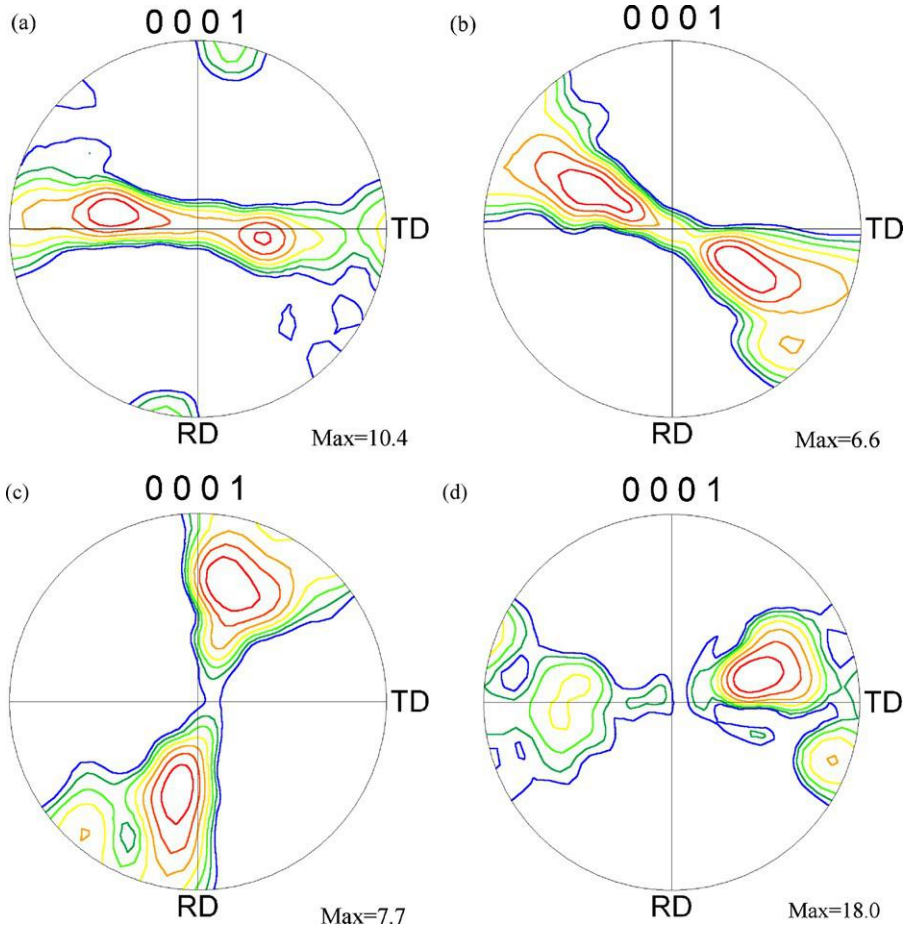

Fig. 10. {0 0 0 1} pole figures of CP Ti during 3/4 ECAP passes at 723 K. (a) Point A, (b) point B, (c) point D and (d) point H.

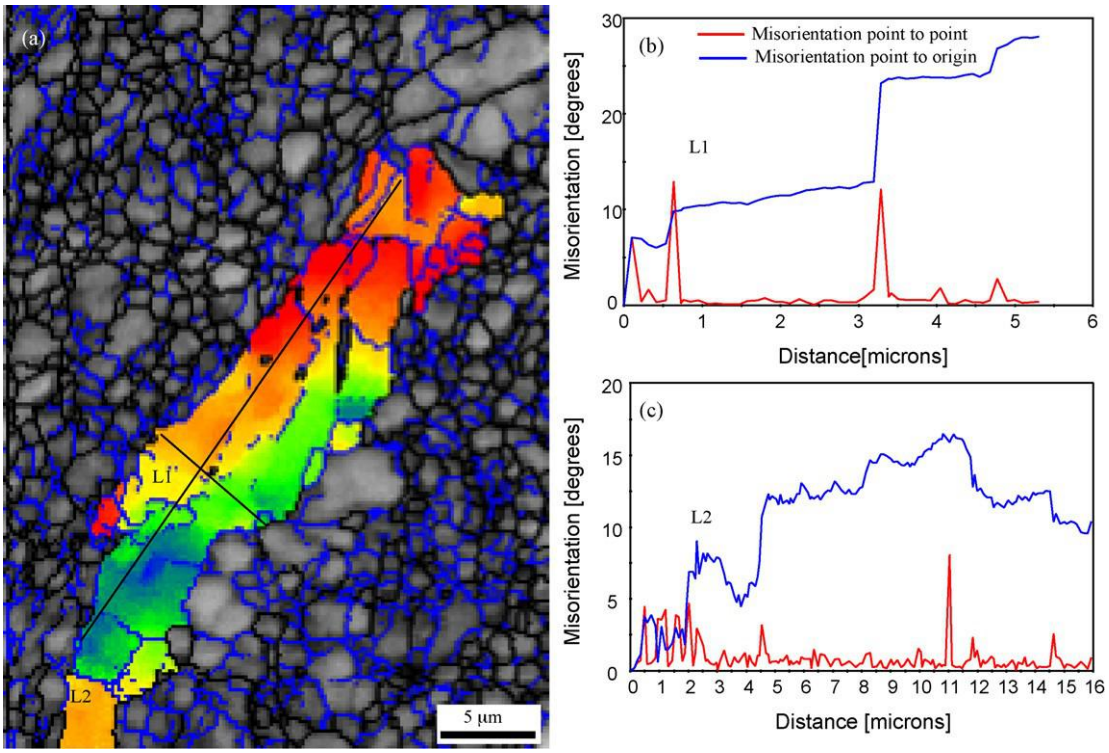

Fig. 11. (a) Highlight from Fig. 6b illustrating the typical misorientation gradient within an elongated coarse grain. L1 and L2 are perpendicular to and parallel to the elongated direction (b) misorientation profile along L1 showing misorientation gradient across the grain and (c) misorientation profile along L2 showing the misorientation gradient along the longitudinal direction.

plotted along two paths, L1 and L2, perpendicular to and parallel to the elongated direction, respectively. The relative misorientation profiles measured along these lines are shown in Fig. 11b and c. The red line and the blue line represent the point-to-point misorientation and the point to origin misorientation, respectively. There are four main misorientation jumps, ranging from 3° to 13°, along L1, located at 0.1, 0.6, 3.3 and 4.8 μm and the maximum accumulated misorientation rises to 28.1° across grain. Along the direction of L2, the point-to-point misorientation generally remains below 5° (Fig. 11c). The accumulated misorientation increases to around 15° over 11 μm from one side of the grain and then decreases progressively approaching the opposite grain boundary. Misorientation gradients have been examined in many coarse grains and one was described in our previous study [13]. Similar long-range misorientation gradients are found in most of the grains: the misorientation gradient across the elongation axis of the coarse grain is larger than that along the longitudinal direction. It can be expected that with further deformation, the coarse, elongated, grains will gradually develop into narrower bands with a larger number of HAGBs. Similar long-range continuous orientation gradients were also reported in torsionally deformed steel and cold rolled aluminum [27,28]. The equivalent geometrically necessary dislocation density can be roughly estimate by the formula, $\rho \approx \theta / b\iota$, where θ is the accumulated in grain misorientation angle, in radians, b is the Burgers vector and ι is the distance [26,27]. Therefore, the higher the ratio between the accumulated misorientation angle and distance, the higher is the dislocation density. Taking $b = 2.95 \times 10^{-10}$ and 5.54×10^{-10} m for $\vec{a}$- and $\vec{a}+\vec{c}$ dislocations in the HCP structure, respectively, $\theta = 28.1°$ (=0.49 rad) and 10.4° (=0.18 rad) for L1 and L2, respectively, $\iota = 5.3 \times 10^{-6}$ m and 15.9×10^{-6} m for L1 and L2, respectively, the estimated local dislocation density becomes 2×10^{14} to 3×10^{14} m^{-2} and 2×10^{13} to 4×10^{13} m^{-2} for the directions of L1 and L2, respectively. This estimated value indicates that the present local dislocation density along L1 is about 10 times of L2 and 2–3 times that of stainless steel after torsion deformation [27].

- Grain refinement mechanism

Continuous dynamic recrystallization (CDRX) occurs easily in pure titanium, due to its high stacking-fault energy [13,29]. The CDRX process is a recovery dominated process and proceeds by continuous absorption of dislocations in subgrain boundaries (LAGBs) which eventually results in the formation of new grains with HAGBs [30]. In our previous work [13], clear evidence of CDRX was seen in the 3/4 passes shear zone. Further microstructural features associated with the operation of CDRX are shown in Fig. 12. The LAGBs and HAGBs are marked by white and black lines in this figure, respectively. Firstly, the large misorientation gradient from the center

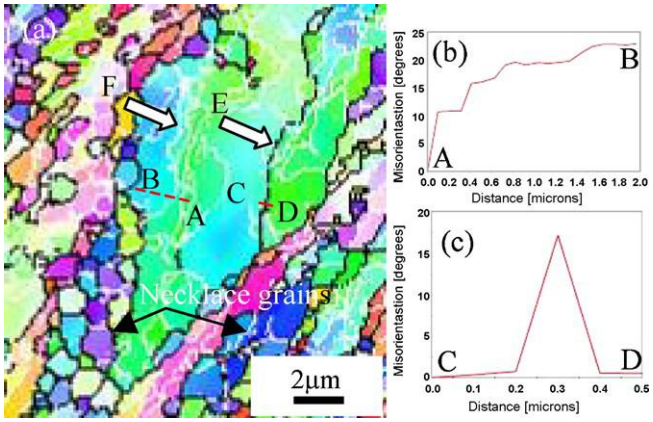

Fig. 12. EBSD orientation map revealing features of CDRX in CP Ti during ECAP, taken from Fig. 6b.

to the grain boundary is frequently observed in coarse grains, as shown in Figs. 12b and Fig. 11. This provides the necessary driving force for the evolution of LAGBs to HAGBs. Secondly, it is apparent that many LAGBs have evolved into HAGBs, see the arrow E in Fig. 12a. Careful inspection of this grain boundary reveals that the misorientation of some segments is just a little higher than the transition value of 15°, used to define a HAGB, Fig. 12c, indicating it is growing by the accumulation of dislocations. Lastly, CDRX is typically identified by the subgrain development around the HAGBs [31,32]. As can be seen in Fig. 12a, most subgrains (LAGBs) are generated near the HAGBs in the original grains and become entangled with each other. With the accumulation of further dislocations, these LAGBs will gradually evolve into HAGBs and form the necklace-like fine grains with HAGBs, marked by arrows in Fig. 12a. The examination of orientation spread inside grains reveals the development of intragranular plastic gradients, substructure, and lattice rotation with respect to the applied route A shear strain. The coarse elongated grains will be refined into narrower band structures as LAGBs (an example marked by arrow F) evolve into HAGBs. With further deformation, all the grains will be refined into necklace-like ultrafine grains by CDRX.

(5) Conclusions

1. A triangular zone showing a different flow line pattern and texture from the other part of the ECAP bar has been found at the extruded end of the sample. The formation of the triangular zone is due to the interaction between the uneven deformation zone at the bar end and the uniform deformation zone in the ECAP bar.
2. The typical microstructure of ECAPed CP Ti after 3 resp. 4 passes via route A contains elongated coarse grains alternating with narrow bands consisting of necklace-like ultrafine equiaxed grains.
3. The deformation of CP Ti during 3 and 4 passes is dominated by dislocation slip. No $\{1\,0\,\bar{1}\,1\}$ twins were detected but a small fraction of $\{1\,0\,\bar{1}\,2\}$ tensile twins were observed to accommodate part of the deformation strain.
4. A detailed misorientation map study shows that long-range misorientation gradients exist in the coarse elongated grains. The misorientation gradients across the deformation bands are much larger than those along the longitudinal direction. With further deformation, the coarse elongated grains will be refined into narrower bands with HAGB structures.
5. The grain refinement mechanism of CP Ti during ECAP has been discussed. The grain refinement of grains in the late passes of ECAP is dominated by CDRX. Most of the ultrafine necklace grains were evolved from subgrains by evolution of LAGBs into HAGBs.

Acknowledgements

The present study was financed by the Norwegian Research Council NANOMAT program. One of the authors (Y.J. Chen) would like to acknowledge the valuable discussion with Prof. J. Hjelen in NTNU.

References

[1] H.J. Rack, J.I. Qazi, Mater. Sci. Eng. C 26 (2006) 1269–1277.
[2] V.V. Stolyarov, Y.T. Zhu, T.C. Lowe, R.Z. Valiev, Mater. Sci. Eng. A 303 (2001) 82–89.
[3] K.S. Raju, M.G. Krishna, K.A. Padmanabhan, K. Muraleedharan, N.P. Gurao, G. Wilde, Mater. Sci. Eng. A (2008), doi:10.1016/j.msea.2007.11.072.
[4] M.P. Liu, H.J. Roven, Y.D. Yu, Int. J. Mater. Res. 98 (2007) 3184–3190.
[5] Y. Miyahara, Z. Horita, T.G. Langdon, Mater. Sci. Eng. A 420 (2006) 240–244.
[6] V.S. Zhernakov, V.V. Latysh, V.V. Stolyarov, A.I. Zharikov, R.Z. Valiev, Scripta Mater. 44 (2001) 1771–1774.
[7] Y.M. Wang, E. Ma, Acta Mater. 52 (2004) 1699–1709.
[8] Y. Fukuda, K. Oh-ishi, Z. Horita, T.G. Langdon, Acta Mater. 50 (2002) 1359–1368.
[9] P.B. Prangnell, A. Gholinia, V.M. Markushev, in: T.C. Lowe, R.Z. Valiev (Eds.), Investigations and Applications of Severe Plastic Deformation, Kluwer Academic Pub., Dordrecht, 2000, p. 65.
[10] X. Zhao, W. Fu, X. Yang, T.G. Langdon, Scripta Mater. 59 (2008) 542–545.
[11] V.V. Stolyarov, Y.T. Zhu, I.V. Alexandrov, T.C. Lowe, R.Z. Valiev, Mater. Sci. Eng. A 343 (2003) 43–50.
[12] S.H. Shin, I. Kim, J. Kim, Y.S. Kim, S.L. Semiatin, Acta Mater. 51 (2003) 983–996.
[13] Y.J. Chen, Y.J. Li, J.C. Walmsley, S. Dumoulin, H.J. Roven, Metall. Trans. A (in press).
[14] Y.T. Zhu, J.Y. Huang, J. Gubicaz, T. Yngar, Y.M. Wang, E. Ma, R.Z. Valiev, J. Mater. Res. 18 (2003) 1908–1916.
[15] M. Furukawa, Y. Iwahashi, Z. Horita, M. Nemoto, T.G. Langdon, Mater. Sci. Eng. A 257 (1998) 328–332.
[16] P. Szczygiel, H.J. Roven, O. Reiso, Mater. Sci. Eng. A 410–411 (2005) 261–264.
[17] Y. Iwahashi, J. Wang, Z. Horita, M. Nemoto, T.G. Langdon, Scripta Mater. 35 (1996) 143–146.
[18] H.J. Roven, S. Dumoulin, J.C. Werenskiold, in: Y.T. Zhu, T.G. Langdon, R.Z. Valiev, S.L. Semiatin, D.H. Shin, T.C. Lowe (Eds.), Ultrafine Grained Materials III, TMS, Philadelphia, USA, 2004, p. 117.
[19] T.G. Langdon, Mater. Sci. Eng. A 462 (2007) 3–11.
[20] Y.T. Zhu, Terry C. Lowe, Mater. Sci. Eng. A 291 (2000) 46–53.
[21] V.M. Segal, Mater. Sci. Eng. A 271 (1999) 322–333.
[22] Y.J. Chen, Q.D. Wang, H.J. Roven, M.P. Liu, M. Karlsen, Y.D. Yu, J. Hjelen, Scripta Mater. 58 (2008) 311–314.
[24] T.A. Mason, J.F. Bingert, G.C. Kaschner, S.I. Wright, R.J. Larsen, Metall. Mater. Trans. A 33 (2002) 949–954.
[25] M.D. Nave, J.J.L. Mulders, A. Gholnia, Chin. J. Stereo. Image Anal. 10 (2005) 199–203.
[26] H. Gao, Y. Huang, Scripta Mater. 48 (2003) 113–118.
[27] D. Jorge-Badiola, A. Iza-Mendia, I. Gutíerrez, Mater. Sci. Eng. A 394 (2005) 445–454.
[28] L. Delannay, O.V. Mishin, D.J. Jensen, P.V. Houtte, Acta Mater. 49 (2001) 2441–2451.
[29] Z. Guo, A.P. Miodownik, N. Saunders, J.-Ph. Schille, Scripta Mater. 54 (2006) 2175–2178.
[30] T. Al-Samman, G. Gottstein, Mater. Sci. Eng. A 490 (2008) 411–420.
[31] A.G. Beer, M.R. Barnett, Metall. Mater. Trans. A 38 (2007) 1856–1867.
[32] F.J. Humphreys, M. Hatherly, Recrystallization and Related Annealing Phenomena, Pergamon, Oxford, United Kingdom, 2004, pp. 427.